Accuracy assessment of the FARO Focus^{3D} and Leica HDS6100 panoramic-type terrestrial laser scanners through point-based and plane-based user self-calibration

Jacky C.K. CHOW, Derek D. LICHTI, and William F. TESKEY, Canada

Key words: Terrestrial laser scanning, calibration, quality assurance, geometric quality, error modelling

SUMMARY

Recent developments of terrestrial laser scanners have made these accurate and efficient survey instruments more affordable and portable. In this paper, the geometric accuracy of two terrestrial laser scanners (i.e. the FARO Focus^{3D} and the Leica HDS6100) is being evaluated. Both of these mid-range instruments are phase-based and have a panoramic architecture. The Focus^{3D} is currently one of the most compact and affordable 3D terrestrial laser scanners on the market. The geometric quality of this latest generation laser scanner will be compared to the HDS6100. The quality assessments performed in this paper are centred on the self-calibration method for terrestrial laser scanners. This method can remove systematic defects in the instrument without hardware modifications or specialized equipment. Through the observation of either signalised targets or planar-features, the residual systematic errors in the laser scanner can be modelled mathematically. From previous studies, these unmodelled systematic errors can drastically deteriorate the point cloud quality and the self-calibration approach has been proven to be an effective tool for eliminating systematic effects caused by flaws of individual components and misalignment between components. Through redundant observations, the distance and angular measurement precision can be estimated in a least-squares adjustment and used as a quantitative measure for comparing the systems. Both laser scanners were tested and calibrated multiple times at the University of Calgary. Based on the experimental results presented in this paper, it was discovered that data coming from the more affordable Focus^{3D} are contaminated with significant systematic errors. Even after self-calibration, the measurement random noise is still higher than the HDS6100. However, at close-range the contribution of the higher random noise to the positioning solution is small and does not have a significant detrimental impact on the mapped scene.

Accuracy assessment of the FARO Focus^{3D} and Leica HDS6100 panoramic-type terrestrial laser scanners through point-based and plane-based user self-calibration

Jacky C.K. CHOW, Derek D. LICHTI, and William F. TESKEY, Canada

1. INTRODUCTION

Terrestrial laser scanning (TLS) instruments have already established their status as a reliable, accurate, and high-speed active 3D mapping solution (Vosselman & Mass, 2010). By measuring spatial distances at uniform increments of arc in two orthogonal directions, 3D coordinates on any laser-suitable surface can be measured without specially-designed targets. In the past, companies have mainly focused on improving the positioning accuracy, acquisition speed, measurable range, and functionalities (e.g. built-in memory storage, Wi-Fi connectivity, built-in batteries, and on-board touch-screen controller) of the scanner. Recently, the cost of 3D terrestrial laser scanners has begun to reduce. Companies such as FARO and Leica are releasing new scanners (i.e. Focus^{3D} and C5, respectively) that are opening new markets to the active 3D imaging industry. Consumers are beginning to find shorter range applications with lower accuracy requirements for these economical laser scanners. In this paper, the geometric accuracy of the FARO Focus^{3D} will be analyzed and compared to a higher accuracy laser scanner from Leica (i.e. the HDS6100). The range, horizontal direction, and elevation angle measurement precision of both instruments were estimated repeatedly using variance component estimations in a point-based user self-calibration routine (Lichti, 2007). Residual systematic errors in both scanners were also recovered and modelled empirically by observing a large quantity of signalised targets or planar-features. Self-calibration is useful because despite the manufacturer's laboratory calibration, systematic errors are still identifiable in various scanners (Kersten et al., 2008) and through self-calibration the geometric accuracy of the scanner can be improved; in some cases improvement from the millimetre level to the sub-millimetre level is possible (Chow et al., 2011b). To assist the point-cloud registration, most modern TLS instruments are equipped with additional sensors for defining the exterior orientation parameters (EOPs) of the instrument, for example built-in electronic compass, dual-axis compensator, and electronic barometer. These additional observations are valuable for reducing correlations between EOPs and the other parameters in the self-calibration adjustment (Lichti, 2010).

2. MATHEMATICAL MODEL

Software calibration of optical sensors is a well-established concept in photogrammetry and computer vision. For analog and digital cameras, bundle adjustment based on the collinearity equations is the preferred self-calibration method for most cases (Brown, 1971). Regarding terrestrial laser scanner self-calibration, registration using 3D rigid body transformation with the observations expressed in the spherical coordinate system has proven to be an effective

approach (Lichti, 2007; Reshetyuk, 2010). In this paper, both the Focus^{3D} and HDS6100 were calibrated using this method but with different geometric primitives. In the point-based self-calibration (Lichti et al., 2007; Reshetyuk, 2009; Schneider, 2009), a large quantity of signalised targets distributed evenly on the walls, ceiling, and floor of a room were observed. These targets, acquired by the scanner occupying different positions and orientations, were then used for registering the point clouds. Additional parameters (APs) were appended to the observation equations to simultaneously correct for biases, axes misalignments, wobbling, etc. As an alternative to the point-based self-calibration approach, well defined geometric features such as lines, planes, cylinders, spheres, and tori can be used to replace signalised targets for registering point clouds and calibrating the scanner. In this paper, besides point-based calibration, planar features were also considered for self-calibration (Bae & Lichti, 2007; Chow et al., 2011a).

2.1 Point-based user self-calibration of terrestrial laser scanners

The point-based self-calibration method is based on the 3D rigid body transformation given in Equation 1. The scanner's range and angles observation with APs appended are shown in Equation 2. The calibration models for range, horizontal direction, and elevation angle observations are given in Equations 3, 4, and 5, respectively. The EOPs of each scanner setup, 3D object space coordinates of every target, and APs are estimated simultaneously in a parametric least-squares adjustment. The stochastic model for the observations is also estimated in the adjustment using variance component estimation. It is assumed that the observations are uncorrelated and the standard deviation of the angular observations is independent of the scanning geometry. The range observations on the other hand are known to vary according to the secant function of the incidence angle (Soudarissanane et al., 2011). The elongation of the laser footprint at large incidence angles causes distance measurements to be integrated over a larger surface area, which results in a lower range measurement precision.

$$\begin{bmatrix} x_{ij} \\ y_{ij} \\ z_{ij} \end{bmatrix} = M_j \left(\begin{bmatrix} X_i \\ Y_i \\ Z_i \end{bmatrix} - \begin{bmatrix} X_{oj} \\ Y_{oj} \\ Z_{oj} \end{bmatrix} \right) \tag{1}$$

$$M_j = R_3(\kappa_j) R_2(\phi_j) R_1(\omega_j)$$

where X_i, Y_i, and Z_i are the object space coordinates of point i.
x_{ij}, y_{ij}, and z_{ij} are the Cartesian coordinates of point i in scanner space j.
X_{oj}, Y_{oj}, and Z_{oj} are the position of scanner j in object space.
ω_j, φ_j, and κ_j are the primary, secondary, and tertiary rotation angles that describes the orientation of scanner j in object space.
R_1, R_2, and R_3 are the rotation matrices about the primary, secondary, and tertiary axis, respectively.

$$\begin{aligned}\rho_{ij} &= \sqrt{x_{ij}^2 + y_{ij}^2 + z_{ij}^2} + \Delta\rho \\ \theta_{ij} &= \tan^{-1}\left(\frac{y_{ij}}{x_{ij}}\right) + \Delta\theta \\ \alpha_{ij} &= \tan^{-1}\left(\frac{z_{ij}}{\sqrt{x_{ij}^2 + y_{ij}^2}}\right) + \Delta\alpha\end{aligned} \tag{2}$$

where, ρ_{ij}, θ_{ij}, and α_{ij} are the range, horizontal circle, and vertical circle reading, respectively to point i in scanner space j
$\Delta\rho$, $\Delta\theta$, and $\Delta\alpha$ are the additional systematic correction parameters for range, horizontal direction, and vertical direction, respectively.

$$\Delta\rho = A_0 + A_1\rho_{ij} + A_2\sin(\alpha_{ij}) + A_3\sin\left(\frac{4\pi}{U_1}\rho_{ij}\right) + A_4\cos\left(\frac{4\pi}{U_1}\rho_{ij}\right) + ET_\rho \tag{3}$$

where A_0 describes the rangefinder offset
A_1 describes the scale factor error
A_2 describes the laser axis vertical offset
A_3 and A_4 describe the cyclic errors
ET_ρ means other empirical range error terms

$$\begin{aligned}\Delta\theta = {} & B_1\theta + B_2\sin(\theta) + B_3\cos(\theta) + B_4\sin(2\theta) + B_5\cos(2\theta) + B_6\sec(\alpha) \\ & + B_7\tan(\alpha) + B_8\rho^{-1} + B_9\sin(\alpha) + B_{10}\cos(\alpha) + ET_\theta\end{aligned} \tag{4}$$

where B_1 describes the scale factor error
B_2 and B_3 describe the horizontal circle eccentricity
B_4 and B_5 describe the non-orthogonality of encoder and vertical axis
B_6 describes the collimation axis error
B_7 describes the trunnion axis error
B_8 describes horizontal eccentricity of collimation axis
B_9 and B_{10} describe the trunnion axis wobble
ET_θ means other empirical horizontal direction error terms

$$\begin{aligned}\Delta\alpha = {} & C_0 + C_1\alpha + C_2\sin(\alpha) + C_3\sin(2\alpha) + C_4\cos(2\alpha) + C_5\rho^{-1} \\ & + C_6\sin(2\theta) + C_7\cos(2\theta) + C_8\sin(4\theta) + ET_\alpha\end{aligned} \tag{5}$$

where C_0 describes the vertical circle index error
C_1 describes the scale factor error
C_2 describes the vertical circle eccentricity
C_3 and C_4 describe the non-orthogonality of encoder and trunnion axis

C_5 describes the vertical eccentricity of collimation axis
C_6, C_7, and C_8 describe the vertical axis wobble
ET_α means the other empirical elevation angle error terms

The centre of each signalised target can be determined using least-squares geometric form fitting or template matching. Typically a laser scanner cannot aim directly at the centre of a target like a total station, therefore an ample amount of observations are made on the surface of the target and the centroid is then calculated precisely by exploiting information/properties about the signalised target such as size, shape, and reflectivity. In cases where the laser scanner was leveled and/or the heading of the scanner was measured, additional observations/constraints can be included in the least-squares adjustment. For example, with the Focus^{3D}, when all three attitude angles are measured internally and applied to the point cloud, the following observations can be added to the adjustment (Equation 6).

$$\begin{aligned} \omega &= \omega_{obs} \pm \sigma_\omega \\ \phi &= \phi_{obs} \pm \sigma_\phi \\ \kappa &= \kappa_{obs} \pm \sigma_\kappa \end{aligned} \tag{6}$$

2.2 Plane-based user self-calibration of terrestrial laser scanners

Instead of a functional model that minimizes the discrepancies of tie points in the X, Y, and Z direction as explained in Section 2.1, a functional model that constrains every point to lie on the best-fit plane is applied instead in the plane-based self-calibration. Although other geometric features can be utilized, planes are beneficial because they are abundant in urban environments, which make in-situ self-calibration more feasible. Following the same rigid body transformation model and spherical parameterization of the observations in Equations 1 and 2, Equation 7 can be adopted to constrain every point to lie on a plane. Instead of estimating the 3D object space coordinates of every target, the plane-based calibration estimates the four plane parameters while minimizing the sum of squares of the residuals. In a combined least-square adjustment, the scanner's EOPs, plane parameters, and APs are all estimated simultaneously.

$$\begin{pmatrix} a_k & b_k & c_k \end{pmatrix} \left\{ M_j \begin{pmatrix} (\rho_{ij} - \Delta\rho)\cos(\alpha_{ij} - \Delta\alpha)\cos(\theta_{ij} - \Delta\theta) \\ (\rho_{ij} - \Delta\rho)\cos(\alpha_{ij} - \Delta\alpha)\sin(\theta_{ij} - \Delta\theta) \\ (\rho_{ij} - \Delta\rho)\sin(\alpha_{ij} - \Delta\alpha) \end{pmatrix} + \begin{pmatrix} X_{o_j} \\ Y_{o_j} \\ Z_{o_j} \end{pmatrix} \right\} - d_k = 0 \tag{7}$$

where a_k, b_k, c_k, d_k are the direction normal and the orthogonal distance to plane k.

3. EXPERIMENT

The Leica HDS6100 was calibrated seven times in the past three years using the point-based self-calibration approach and four times using the plane-based self-calibration method. Self-calibration was carried out for the newer Focus^{3D} six times using the point-based method and once using the plane-based method this year. The calibrations were all performed at the University of Calgary in one of two rooms. The smaller room (Figure 1) has dimensions 5 m by 5 m by 3 m and the larger room (Figure 2) is 14 m by 11 m by 3 m. In both situations, either a redundant number of targets were observed or a redundant number of planes were observed. For the point-based calibration either circular or checkerboard type paper targets were deployed and their centroids were determined using least-squares geometric form-fitting as explained in Chow et al. (2010) and Chow et al. (2011b), respectively. In the plane-based self-calibration, besides natural planes in the environment (i.e. walls) additional metal plates with a glossy white finish were introduced to strengthen the network geometry. The number of scans, number of targets/planes, number of observations, number of unknowns, and the average redundancy for the HDS6100 and Focus^{3D} calibrations are summarized in Tables 1 and 2, respectively.

Figure 1: Small 5 x 5 x 3m calibration room

Figure 2: 14 x 11 x 3m Large calibration room

Table 1: Summary of some statistics from the HDS6100 self-calibrations

Dataset	Room	Point/plane based	# of scans	# of targets/planes	# of obs.	# of unk.	Avg. Red.
1	Small	Point	6	264	3495	833	0.76
2	Large	Point	6	63	759	231	0.70
3	Large	Point	6	63	762	230	0.70
4	Large	Point	4	102	963	335	0.66
5	Large	Point	4	104	837	339	0.60
6	Small	Point	4	181	2069	571	0.73
7	Large	Point	6	300	3591	936	0.74
8	Large	Plane	6	9	43137	75	0.33
9	Large	Plane	6	9	40653	74	0.33
10	Large	Plane	4	70	33900	308	0.33
11	Large	Plane	4	60	28194	268	0.33

Table 2: Summary of some statistics from the Focus^{3D} self-calibrations							
Dataset	**Room**	**Point/plane based**	**# of scans**	**# of targets/planes**	**# of obs.**	**# of unk.**	**Avg. Red.**
1	Small	Point	4	206	1833	646	0.65
2	Small	Point	4	183	2001	573	0.72
3	Small	Point	4	176	2040	557	0.73
4	Small	Point	4	166	1821	526	0.71
5	Large	Point	7	300	3786	942	0.75
6	Large	Point	7	300	3429	942	0.73
7	Small	Plane	4	52	31200	235	0.33

4. RESULTS & ANALYSES

Non-random trends due to systematic defects can usually be visually identified in the residuals when plotted versus the scanner's raw observations. For instance, significant trunnion axis error and collimation axis error were observed in calibration dataset 2 for the Focus^{3D} (Figure 3).

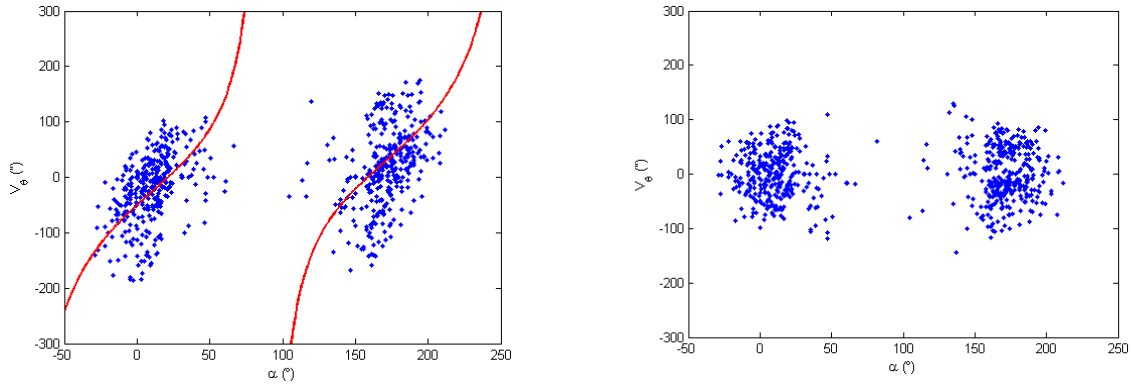

(a) *(b)*

Figure 3: Residuals of the horizontal circle reading as function of the elevation angle (a) ***before*** *self-calibration and (b)* ***after*** *self-calibration.*

The estimated raw observation precision of both scanners before and after applying the point-based self-calibration is given in Figure 4. The average σ_ρ, σ_θ, and σ_α before and after point-based self-calibration for the HDS6100 and Focus^{3D} are shown in Table 3. It is evident that in general the calibration routine can help improve the observation precision of the scanner and the standard deviation of the HDS6100's observations are in general half of the Focus^{3D}. The estimated range precision of the HDS6100 is comparable to the independent accuracy assessment carried out in Nuttens et al. (2010). It is worthwhile mentioning that the HDS6100 was sent back to the manufacturer for repairs after dataset 1. It is evident from Figure 4 that after the manufacturer's precise laboratory calibration, the noise level of the instrument was reduced, but it was still improved further using the self-calibration method. As the scanner experiences wear and tear, the HDS6100's elevation angle measurement precision declined over time and reached the same level of precision as the Focus^{3D}.

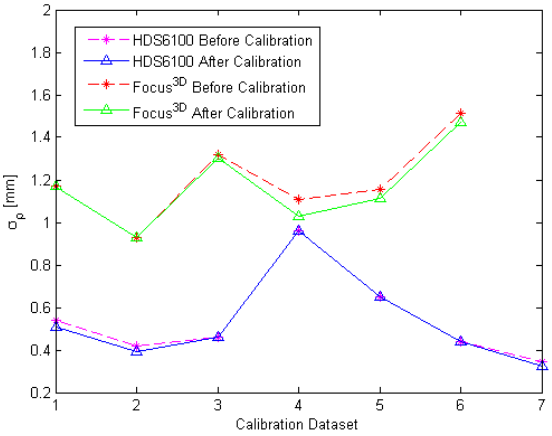

(a)

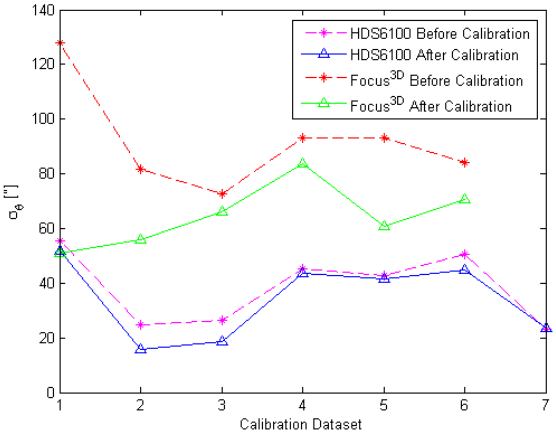

(b)

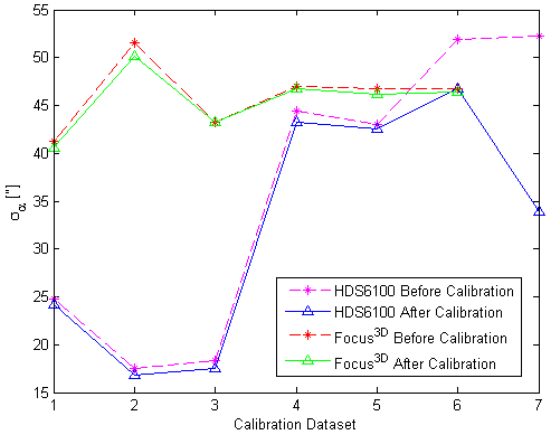

(c)

*Figure 4: (a) Estimated **range** observation precision for the HDS6100 and Focus^{3D} before and after point-based self-calibration. (b) Estimated **horizontal circle** observation precision for the HDS6100 and Focus^{3D} before and after point-based self-calibration. (c) Estimated **elevation angle** observation precision for the HDS6100 and Focus^{3D} before and after point-based self-calibration.*

Table 3: Average observation standard deviation before and after point-based self-calibration

	HDS6100			Focus^{3D}		
	Before	After	Improv.	Before	After	Improv.
σ_ρ [mm]	0.55	0.53	2.2%	1.20	1.17	2.6%
σ_θ ["]	38.4	34.2	11.0%	92.0	64.8	29.6%
σ_α ["]	36.0	32.1	10.8%	46.1	45.6	1.1%

The recovered systematic errors that are either statistically significant and/or observable in the range, horizontal direction, and elevation angle residual plots are shown in Tables 4 and 5 for the HDS6100 and the Focus^{3D}, respectively. Even though residual systematic errors can be observed in most modern TLS instruments they might be small for some scanners. On the contrary, it can be argued that self-calibration is more essential for older or low-cost scanners because they appear to exhibit more significant residual systematic errors. The trunnion axis error and collimation axis error in the Focus^{3D} are the most significant, and after calibration improvements up to 60% in the horizontal direction measurement precision can be observed. If not modelled properly, a 100 arcsec trunnion axis error and 100 arcsec collimation axis

error can result in a horizontal error of -5 mm and 7 mm, respectively at a 45^o elevation angle and 10 m distance from the scanner. The reason behind the fluctuation of the scanner's APs is unknown; it might be due to the scanner's instability and/or temperature changes internal to the instrument (Glennie & Lichti, 2011). But as explained in Habib & Morgan (2005) and Lichti (2008), there are some shortfalls when directly comparing APs for checking temporal stability.

Table 4: Recovered systematic errors for the HDS6100 through point-based and plane-based self-calibration

Dataset	A_0	A_2	B_2	B_3	B_4	B_5	B_6	B_7	C_0	C_6	C_7	C_8
1	-1.08 ± 0.09						11.0 ± 1.8	-18.0 ± 3.7	-50.5 ± 8.3			
2	-0.83 ± 0.16		24.0 ± 3.8		-10.7 ± 1.6			-22.7 ± 3.9	-34.0 ± 9.9			6.2 ± 1.6
3	-1.1 ± 0.20		26.2 ± 0.53		-9.6 ± 2.2			-29.0 ± 5.4	-27.2 ± 13.1			
4	-0.57 ± 0.25				-11.6 ± 3.6	-12.3 ± 3.6				-9.0 ± 3.6	-7.5 ± 3.6	
5		1.76 ± 0.47			-9.1 ± 3.8	-14.1 ± 3.6						
6						-17.4 ± 4.7	-14.6 ± 4.2	-49.5 ± 10.4				
7	-0.42 0.05						-2.0 0.9	-40.7 1.7	-117.2 4.0			
8	-2.12 ± 0.19					11.4 ± 3.4		-28.9 ± 15.9				
9	-1.99 ± 0.20			-16.3 ± 3.1								
10	-0.94 ± 0.08						-6.6 ± 1.6	-26.5 ± 10.6	8.9 ± 2.4			
11	0.52 ± 0.12							-50.9 ± 10.8	10.3 ± 2.5			

Table 5: Recovered systematic errors for the Focus^{3D} through point-based and plane-based self-calibration

Dataset	A_0	B_2	B_3	B_4	B_5	B_6	B_7	C_0	C_3	C_7
1				13.6 ± 3.1	10.9 ± 3.2	87.4 ± 4.5	-203.8 ± 8.8			
2	0.54 ± 0.23	-27.5 ± 9.2	-51.8 ± 3.6			50.3 ± 2.9	-138.3 ± 6.8		24.2 ± 4.4	
3	1.12 ± 0.23					49.6 ± 4.8	-32.6 ± 9.8			12.3 ± 2.8
4	2.12 ± 0.31		-54.5 ± 5.2				44.2 ± 9.8			
5	0.48 ± 0.18					58.1 ± 2.2	-49.6 ± 3.6	-37.3 ± 7.5		
6	0.96 ± 0.23					50.2 ± 2.7	-59.1 ± 4.1	-38.9 ± 8.1		
7	2.02 ± 0.42					102.0 ± 6.5	-113.3 ± 17.7	128.7 ± 13.0		

Although the estimated standard deviation of the observations is a valid approach to compare

the two instruments, in most cases the user is only concerned about the object space accuracy. To assess the difference in the reconstructed object space by the two scanners, a check point analysis was performed. The HDS6100 and Focus^{3D} were calibrated in the same room on the same day and the determined object space coordinates from both adjustments were compared. In the small room, 168 targets from dataset 6 of the HDS6100 and dataset 3 of the Focus^{3D} were compared. In the large room, 200 targets from dataset 7 of the HDS6100 and dataset 5 of the Focus^{3D} were compared. The object space coordinates determined by both scanners were transformed into a common coordinate system using a 7-parameter 3D similarity transformation. The computed RMSE of the targets before and after self-calibration in the X, Y, and Z directions are shown in Table 6. This check point analysis indicates high compatibility between the two scanners. In the small room, the overall differences between the target positions are less than a millimeter in all directions. At larger distances, the effect of the angular systematic errors is more pronounced, and after self-calibration the compatibility between the point clouds acquired by the HDS6100 and Focus^{3D} was improved.

Table 6: Differences between the signalised target positions determined by the HDS6100 and Focus^{3D}

	Before Calibration [mm]			After Calibration [mm]		
Room	$RMSE_X$	$RMSE_Y$	$RMSE_Z$	$RMSE_X$	$RMSE_Y$	$RMSE_Z$
Small	0.7	0.8	0.5	0.7	0.7	0.5
Large	0.6	0.8	2.2	0.5	0.8	1.4

Systematic artifacts can be observed in the Focus^{3D} point cloud as shown in Figures 5 and 6a. Near the zenith, a hole in the data can be observed. At low elevations, a mismatch between the point clouds measured on the floor captured in face 1 and face 2 is apparent. After calibration in dataset 7, the 5 mm horizontal displacement between the data captured in front and behind the sensor is eliminated as shown in Figure 6. Note that when capturing a 360^o scan, data from face 1 and face 2 overlapped, this is probably because the instrument scanned beyond 360^o. For the analysis shown in Figure 6, the overlapping points are removed. The hole on the ceiling situated 1.7 m above the scanner has a maximum diameter of approximately 1.3 cm before calibration and 1.2 cm after calibration. Future work will attempt to improve the self-calibration method and eliminate this systematic defect near zenith.

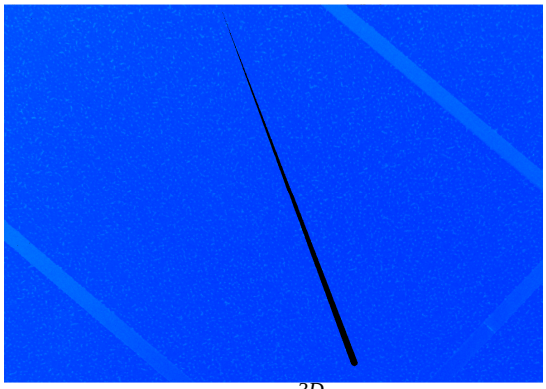

Figure 5: A hole in the Focus^{3D} point cloud near zenith

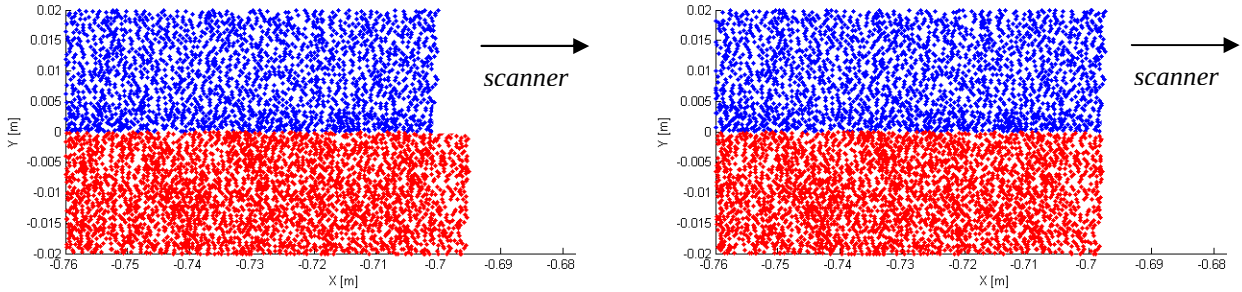

(a) (b)

*Figure 6: Top view of the displacement between face 1 scan data (blue) and face 2 scan data (red) at low elevation angles near the tripod (a) **before** calibration and (b) **after** calibration in scanner space*

5. CONCLUSION

The geometric quality of the point clouds acquired by two different scanners (i.e. a Leica HDS6100 and a FARO Focus^{3D}) was compared quantitatively in this paper. Independent point-based and plane-based self-calibrations were carried out for both sensors to study their systematic errors and raw observation precision. The object space reconstructed by both scanners was also compared directly to evaluate the geometric performance of the more affordable Focus^{3D}. From the empirical data, it was discovered that the point clouds generated by both scanners were contaminated by unmodelled systematic errors. The Focus^{3D} showed significant systematic errors in the horizontal circle measurements in all cases. The HDS6100's observation quality appears to be deteriorating slightly, perhaps due to wear and tear, especially in the elevation angle measurements. Even after the residual systematic errors have been modelled using the self-calibration method, the random noise of the Focus^{3D}'s observations remains approximately twice the magnitude of that of the HDS6100. However, in close-range, it has been demonstrated in this paper that the discrepancy in the reconstructed object space is small and negligible for most applications. At longer ranges, self-calibration has advantages in improving the geometric accuracy of the reconstructed environment. Future work will attempt to improve the self-calibration technique to remove the systematic artifacts near the zenith.

ACKNOWLEDGEMENTS

Research funding provided by the Natural Sciences and Engineering Research Council of Canada, the Canada Foundation for Innovation, Alberta Innovates, Informatics Circle of Research Excellence, Terramatic Technologies Inc., and SarPoint Engineering Ltd. is gratefully acknowledged. The authors are sincerely appreciative for the help they have received when setting up the experiments and collecting the data; thank you Axel Ebeling, Ivan Detchev, Claudius Schmitt, John Tang, and Kathleen Ang.

REFERENCES

Bae, K., & Lichti, D. (2007). On-site self-calibration using planar features for terrestrial laser scanners. *The international Archives of the Photogrammery, Remote Sensing and Spatial Information Sciences 36 (Part 3/W52)*, 14-19.

Brown, D. (1971). Close-range camera calibration. *Photogrammetric Engineering, 37 (8)*, 855-866.

Chow, J., Ebeling, A., & Teskey, W. (2010). Low Cost Artificial Planar Target Measurement Techniques for Terrestrial Laser Scanning. *FIG Congress 2010: Facing the Challenges - Building the Capacity.* Sydney, Australia, April 11-16.

Chow, J., Lichti, D., & Glennie, C. (2011a). Point-based versus plane-based self-calibration of static terrestrial laser scanners. *ISPRS Laser Scanning Workshop 2011*. Calgary, Canada.

Chow, J., Teskey, W., & Lovse, J. (2011b). In-situ self-calibration of terrestrial laser scanners and deformation analysis using both signalized targets and intersection of planes for indoor applications. *Joint International Symposium on Deformation Monitoring.* Hong Kong, China.

Glennie, C., & Lichti, D. (2011). Temporal stability of the Velodyne HDL-64E S2 scanner for high accuracy scanning applications. *Remote Sensing 3(3)*, 539-553.

Habib, A., & Morgan, M. (2005). Stability analysis and geometric calibration of off-the-shelf digital cameras. *Photogrammetric Engineering and Remote Sensing 71(6)*, 773-741.

Kersten, T., Mechelke, K., Lindstaedt, M., & Sternberg, H. (2008). Geometric Accuracy Investigations of the Latest Terrestrial Laser Scanning Systems. *FIG Working Week: Integrating Generations.* Stockholm, Sweden 14-19 June 2008.

Lichti, D. (2007). Modelling, calibration and analysis of an AM-CW terrestrial laser scanner. *ISPRS Journal of Photogrammetry and Remote Sensing 61 (5)*, 307-324.

Lichti, D. (2008). A method to test differences between additional parameter sets with a case study in terrestrial laser scanner self-calibration stability analysis. *ISPRS Journal of Photogrammetry and Remote Sensing, 63 (2)*, 169-180.

Lichti, D. (2010). Terrestrial laser scanner self-calibration: correlation sources and their mitigation. *ISPRS Journal of Photogrammetry and Remote Sensing 65 (1)* , 93-102.

Lichti, D., Brustle, S., & Franke, J. (2007). Self-calibration and analysis of the Surphaser 25HS 3D scanner. *Strategic Integration of Surveying Services, FIG Working Week 2007.* Hong Kong, China: May 13-17, 2007.

Nuttens, T., De Wulf, A., Bral, L., De Wit, B., Carlier, L., De Ryck, M., et al. (2010). High resolution terrestrial laser scanning for tunnel deformation measurements. *FIG Congress 2010: Facing the Challenges - Building the Capacity.* Sydney, Austrailia, April 11-16.

Reshetyuk, Y. (2009). Self-calibration and direct georeferencing in terrestrial laser scanning. *Doctoral Thesis. Department of Transport and Economics, Division of Geodesy, Royal Institute of Technology (KTH), Stockholm, Sweden, January.*

Reshetyuk, Y. (2010). A unified approach to self-calibration of terrestrial laser scanners. *ISPRS Journal of Photogrammetry and Remote Sensing 65 (5)* , 445-456.

Schneider, D. (2009). Calibration of a Riegl LMS-Z420i based on a multi-station adjustment and a geometric model with additional parameters. *The International Archives of the Photogrammetry, Remote Sensing and Spatial Information Sciences 38 (Part 3/W8)*, 177-182.

Soudarissanane, S., Lindenbergh, R., Menenti, M., & Teunissen, P. (2011). Scanning geometry: Influencing factor on the quality of terrestrial laser scanning points. *ISPRS Journal of Photogrammetry and Remote Sensing 66(4)*, 389–399.

Vosselman, G., & Maas, H.-G. (2010). *Airborne and Terrestrial Laser Scanning.* Scotland, UK: Whittles Publishing.

BIOGRAPHICAL NOTES

Jacky is currently a PhD student studying Geomatics Engineering at the University of Calgary. He specializes in close-range photogrammetry, digital imaging techniques, and deformation monitoring. His research interests include: image sensor error modelling (e.g. self-calibration of terrestrial laser scanners, digital medium format cameras, and 3D range cameras), point cloud manipulation and processing (e.g. geometric form fitting, feature extraction, segmentation, filtering, and classification), markerless point cloud registration techniques (e.g. ICP), multi-sensor integration, biomedical imaging, and simultaneous localisation and mapping, mocap, and inertial measurements.

Dr. Derek Lichti is currently Associate Professor in the Department of Geomatics Engineering at the University of Calgary, Canada, and Chair (2008-2012) of the International Society for Photogrammetry and Remote Sensing (ISPRS) Working Group V/3 *Terrestrial Laser Scanning and 3D Imaging*. His research activities focus on the modeling and use of optical and range imaging sensors for automated 3D object reconstruction for a broad spectrum of applications including structural measurement, mobile mapping and human-computer interaction.

Dr. William (Bill) Teskey is a Professor in the Department of Geomatics Engineering at the University of Calgary. He is a registered Professional Engineer in Alberta and a registered Land Surveyor in Alberta and Canada. Bill served for a number of years on the Western Canadian Board of Examiners for Land Surveyors and on the Board of Examiners of the Association of Professional Engineers, Geologists and Geophysicists of Alberta. His areas of interest are precise engineering and deformation surveys.

CONTACTS

Jacky C.K. Chow
Department of Geomatics Engineering
Schulich School of Engineering, University of Calgary
2500 University Drive N.W.
Calgary, Alberta, T2N 1N4
Canada
Tel: +1 (403) 220-3582
Fax: + 1 (403) 284-1980
Email: jckchow@ucalgary.ca

Prof. Dr. Derek D. Lichti
Department of Geomatics Engineering
Schulich School of Engineering, University of Calgary
2500 University Drive N.W.
Calgary, Alberta, T2N 1N4
Canada
Tel: +1 (403) 210-9495
Fax: +1 (403) 284-1980
Email: ddlichti@ucalgary.ca

Prof. Dr. William F. Teskey
Department of Geomatics Engineering
Schulich School of Engineering, University of Calgary
2500 University Drive N.W.
Calgary, Alberta, T2N 1N4
Canada
Tel: +1 (403) 220-7397
Fax: + 1 (403) 284-1980
Email: wteskey@ucalgary.ca